European Journal of Computational Mechanics
Vol. 21, Nos. 1–2, February–April 2012, 92–102

Taylor & Francis
Taylor & Francis Group

Polygonal finite elements for three-dimensional Voronoi-cell-based discretisations

Kaliappan Jayabal[a]* and Andreas Menzel[a,b]

[a]*Institute of Mechanics, TU Dortmund, Leonhard-Euler-Str. 5, D 44227 Dortmund, Germany;* [b]*Division of Solid Mechanics, Lund University, P.O. Box 118, SE 221 00 Lund, Sweden*

Hybrid finite element formulations in combination with Voronoi-cell-based discretisation methods can efficiently be used to model the behaviour of polycrystalline materials. Randomly generated three-dimensional Voronoi polygonal elements with varying numbers of surfaces and corners in general better approximate the geometry of polycrystalline micro- or rather grain-structures than the standard tetrahedral and hexahedral finite elements. In this work, the application of a polygonal finite element formulation to three-dimensional elastomechanical problems is elaborated with special emphasis on the numerical implementation of the method and the construction of the element stiffness matrix. A specific property of Voronoi-based discretisations in combination with a hybrid finite element approach is investigated. The applicability of the framework established is demonstrated by means of representative numerical examples.

L'utilisation d'une formulation hybride en éléments finis combinée à une discrétisation basée sur la méthode de génération de cellules de Voronoi permet d'analyser de manière efficace le comportement des matériaux polycristallins. La génération aléatoire, par la méthode de Voronoi, d'éléments tridimensionnels polygonaux avec un nombre variable de surfaces et de coins permet généralement de mieux approximer la forme des grains que par l'utilisation d'éléments finis standard tétraédriques ou hexaédriques. Dans cette étude, l'application aux problèmes élastiques d'une formulation utilisant des éléments finis polygonaux est développée. Une attention particulière est donnée à l'implémentation numérique et à la construction de la matrice de rigidité d'un élément polygonal. En particulier, la propriété spécifique d'une discrétisation basée sur la méthode de Voronoi combinée à une formulation éléments finis hybrides est étudiée. L'applicabilité et la pertinence de l'approche proposée sont démontrées sur des exemples numériques détaillés dans ce papier.

Keywords: polygonal finite elements; hybrid finite element method; three-dimensional Voronoi cells; stress approximation

Mots-clés: polygonal finite elements; hybrid finite element method; three-dimensional Voronoi cells; stress approximation

1. Introduction

Finite element methods are nowadays well established to efficiently solve inhomogeneous boundary value problems. In case specific geometries or micro-structures are discretised, special finite elements may increase the numerical performance of the simulation. In view

*Corresponding author. Email: jayabal.kaliappan@udo.edu

ISSN 1779-7179 print/ISSN 1958-5829 online

http://dx.doi.org/10.1080/17797179.2012.702432
http://www.tandfonline.com

of the modelling and simulation of the micro-structure of polycrystalline materials, naturally evolving Voronoi polygonal discretisations in general better or rather more efficiently represent the grain and subgrain structure than standard tetrahedrons and hexahedrons. Three-dimensional Voronoi polygons may possess a randomly varying number of surfaces, say 4–20, and corners, say 4–30. It is obvious that a discretisation by means of fine mesh with standard finite elements significantly increase the computational costs. Hybrid finite elements, however, may show an improved performance as the approximation of the stresses within the element is improved. In contrast, the displacements may be approximated only along the element boundaries. Such an approach, first established by Pian (1964) was exploited for two-dimensional Voronoi polygonal elements by Ghosh and Mallett (1994) and Ghosh and Moorthy (1995) later on. A three-dimensional Voronoi-cell finite element model was developed by Ghosh and Moorthy (2004), with application to heterogeneous materials containing a dispersion of ellipsoidal inclusions or voids in the ambient matrix material. The two-dimensional Voronoi-based discretisations combined with the hybrid finite element method, which is also referred here to as the polygonal finite element method (PolyFEM), were studied for the coupled electromechanical cases, in particular ferroelectrics, by Jayabal, Menzel, Arockiarajan, and Srinivasan (2011) and Sze and Sheng (2005). Specific properties of such two-dimensional Voronoi discretisations for the PolyFEM are also discussed by Jayabal and Menzel (2011). The choice of the stress approximation functions within the polygonal finite elements can be based on the type of displacement approximation functions along the element edges regardless of the number of nodes of the respective polygonal finite element, (cf. Jayabal & Menzel, 2011) with application to two-dimensional mechanical and electromechanical problems.

In this work, the PolyFEM is applied to three-dimensional Voronoi-cell-based discretisations for elasto-mechanical problems. In particular, aspects of numerical implementation are discussed and specific advantages of combining the PolyFEM with Voronoi-cell-based meshes are studied. The paper is organised as follows: Section 2 deals with the formulation of the PolyFEM and the underlying element stiffness matrix. Aspects of numerical implementation of the PolyFEM in combination with the Voronoi-cell-based meshes are discussed in Section 3. Some numerical examples for the mechanical problems are presented in Section 4 and the paper concludes with a summary in Section 5.

2. Element formulation for the PolyFEM

The discrete Hellinger–Reissner functional Π for standard continuum undergoing small strains can – with application of the divergence theorem and making use of the quasi-static balance of linear momentum form with volume forces being neglected – be expressed as

$$\Pi_e = \int_{\partial\mathcal{B}_e} [\boldsymbol{n}\cdot\boldsymbol{\sigma}]\cdot\boldsymbol{u}\,\mathrm{d}a - \int_{\mathcal{B}_e} \tfrac{1}{2}\boldsymbol{\sigma} : \mathsf{C} : \boldsymbol{\sigma}\,\mathrm{d}v - \int_{\partial\mathcal{B}_e^t} \bar{\boldsymbol{t}}\cdot\boldsymbol{u}\,\mathrm{d}a \tag{1}$$

wherein $\mathcal{B}_e$ represents a discrete Voronoi-cell-based polygonal finite element. Moreover, $\boldsymbol{u}$ are the displacements, $\boldsymbol{\sigma}$ represents the symmetric stresses, $\boldsymbol{n}$ denotes the outward unit normal vector with respect to the element surfaces, C is the compliance tensor and $\bar{\boldsymbol{t}}$ characterises the prescribed surface traction on $\partial\mathcal{B}_e^t$.

It becomes obvious from Equation (1) that $\boldsymbol{\sigma}$ must be approximated within the volume of the element ($\mathcal{B}_e$), while $\boldsymbol{u}$ is to be defined only along the element surfaces ($\partial\mathcal{B}_e$), (cf. Ghosh & Mallett, 1994; Jayabal et al., 2011). A polygonal finite element can possess any number of surfaces and the continuity conditions for $\boldsymbol{u}$ are to be satisfied across these surfaces between

the adjacent elements. Hence, the stresses – here also expressed in Voigt notation, $\boldsymbol{\sigma}^{\text{voi}} = [\sigma_{xx}\ \sigma_{yy}\ \sigma_{zz}\ \sigma_{yz}\ \sigma_{xz}\ \sigma_{xy}]^{\text{t}}$ – and the displacements can be defined, respectively, within the element and on the element boundary by

$$\boldsymbol{\sigma}^{\text{voi}} = \boldsymbol{M} \cdot \boldsymbol{\beta}_e \quad \text{and} \quad \boldsymbol{u} = \boldsymbol{N} \cdot \boldsymbol{q}_e, \tag{2}$$

where $\boldsymbol{M}$ and $\boldsymbol{N}$ include the approximation functions for $\boldsymbol{\sigma}$ and $\boldsymbol{u}$, with $\boldsymbol{\beta}_e$ and $\boldsymbol{q}_e$ being the corresponding stress coefficients and the nodal displacement degrees of freedom respectively. In other words, the polynomial functions in $\boldsymbol{M}$, that are expressed in terms of the local coordinates of the element, define the stress in the volume of the element, whereas the polynomial functions in $\boldsymbol{N}$ interpolate the displacements only on the element surfaces. Combining Equations (1) and (2), the potential Π can be expressed in a more compact form as

$$\Pi_e = \boldsymbol{\beta}_e \cdot \boldsymbol{G}_e \cdot \boldsymbol{q}_e - \frac{1}{2}\boldsymbol{\beta}_e \cdot \boldsymbol{J}_e \cdot \boldsymbol{\beta}_e - \boldsymbol{q}_e \cdot \boldsymbol{f}_e, \tag{3}$$

where

$$\boldsymbol{G}_e = \int_{\partial \mathcal{B}_e} \boldsymbol{M}^{\text{t}} \cdot [\boldsymbol{n} \cdot \boldsymbol{N}]\ \text{d}a, \tag{4a}$$

$$\boldsymbol{J}_e = \int_{\mathcal{B}_e} \boldsymbol{M}^{\text{t}} \cdot \mathbf{C}^{\text{voi}} \cdot \boldsymbol{M}\ \text{d}v, \tag{4b}$$

$$\boldsymbol{f}_e = \int_{\partial \mathcal{B}_e^t} \boldsymbol{N} \cdot \bar{\boldsymbol{t}}\ \text{d}a. \tag{4c}$$

The stationary of Π in Equation (3) with respect to $\boldsymbol{\beta}_e$ ends – at the element level – up with

$$\boldsymbol{\beta}_e = \boldsymbol{J}_e^{-1} \cdot \boldsymbol{G}_e \cdot \boldsymbol{q}_e \tag{5}$$

which, on substituting this result into the same equation, renders

$$\Pi_e = \frac{1}{2}\boldsymbol{q}_e \cdot \boldsymbol{G}_e^{\text{t}} \cdot \boldsymbol{J}_e^{-1} \cdot \boldsymbol{G}_e \cdot \boldsymbol{q}_e - \boldsymbol{q}_e \cdot \boldsymbol{f}_e. \tag{6}$$

The stationary of Π in the form of Equation (6) with respect to $\boldsymbol{q}_e$ provides the set of linear equation common for standard finite elements formulation in linear elasticity, i.e.

$$\mathbf{A}_e\, \boldsymbol{K}_e \cdot \boldsymbol{q}_e = \mathbf{A}_e \boldsymbol{f}_e \qquad \text{with} \qquad \boldsymbol{K}_e = \boldsymbol{G}_e^t \cdot \boldsymbol{J}_e^{-1} \cdot \boldsymbol{G}_e, \tag{7}$$

and the notation $\mathbf{A}$ denotes the assembly operator. After the nodal degrees of freedom, in other words the displacements at the element nodes $\boldsymbol{q}_e$, are evaluated from Equation (7), the flux coefficients of the element $\boldsymbol{\beta}_e$ can be determined from Equation (5). With the element stresses evaluated by Equation (2), the strains $\boldsymbol{\varepsilon}$ can be calculated from the constitutive relation, $\boldsymbol{\varepsilon} = \mathbf{C} : \boldsymbol{\sigma}$.

3. Numerical Implementation

Preliminary to employing the PolyFEM, a discretisation of the configuration of the body of interest is performed, whereby we make use of Voronoi polygons. Given a set of random points, a three-dimensional Voronoi mesh can be generated as documented in, for instance, Aurenhammer (1991) and references cited therein. An example of such a mesh generated by means of 100 randomly initialised points is shown in Figure 1(a). The total number of elements corresponds to the number of randomly generated points whereas the total number of element nodes varies depending on the position of the randomly generated points. A Voronoi polygonal element within the mesh plotted in Figure 1(a), here possessing 17 surfaces and 29 nodes, is shown in Figure 1(b).

Apart from the discretisation itself, one has to introduce approximation functions $\boldsymbol{M}$ for stresses that enable to fulfil the equilibrium conditions. To ensure invariance, $\boldsymbol{M}$ can be chosen such that it consists of complete polynomial terms. In addition, the choice of $\boldsymbol{M}$ should guarantee the stiffness matrix turns out to be rank sufficient. The following equation provides the related necessary but not sufficient condition for $\boldsymbol{K}_e$, i.e.

$$m \geqslant i * d - r \,, \tag{8}$$

where m, i, d and r refer to, respectively, the rank of the element stiffness matrix, the number of nodes in the polygonal finite element, the degree of freedom per node and the number of rigid body modes of the element. For three-dimensional problems, d becomes three denoting the displacements along the x-, y- and z-axes and r takes the value of six, namely three translations and three rotations. The following stress approximation function

$$\boldsymbol{M} = \left[\begin{array}{c|cccccccccccc} & 2x & 0 & 0 & y & 0 & 0 & z & 0 & 0 & 0 & 0 & 0 \\ & 0 & 2y & 0 & 0 & z & 0 & 0 & x & 0 & 0 & 0 & 0 \\ \boldsymbol{I}_{6\times 6} & 0 & 0 & 2z & 0 & 0 & x & 0 & 0 & y & 0 & 0 & 0 \\ & 0 & -z & -y & 0 & 0 & 0 & 0 & 0 & 0 & x & 0 & 0 \\ & -z & 0 & -x & 0 & 0 & 0 & 0 & 0 & 0 & 0 & y & 0 \\ & -y & -x & 0 & 0 & 0 & 0 & 0 & 0 & 0 & 0 & 0 & z \end{array} \right] , \tag{9}$$

where $\boldsymbol{I}_{6\times 6}$ denotes the identity matrix, may render $\boldsymbol{K}_e$ to be rank sufficient for a hexahedral element together with a proper integration scheme. If a discretisation consists exclusively of

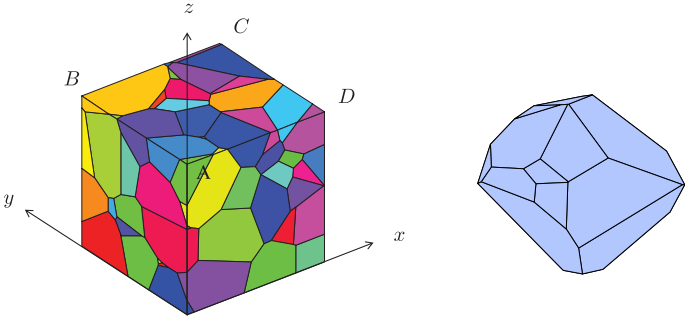

Figure 1. (a) Voronoi-based discretisation of a volume domain by 100 polygonal elements and (b) a polygonal finite element within the mesh consisting 17 faces and 29 nodes.

hexahedral or tetrahedral polygons, $\boldsymbol{M}$ in the form given in Equation (9) can be used for all elements. This renders the individual stiffness matrices as well as the global stiffness matrix to be rank sufficient. As seen in Figure 1, however, the polygonal finite elements in a general Voronoi-cell-based discretisation possess varying numbers of surfaces and nodes. It turns out that making use of $\boldsymbol{M}$ in the form of Equation (9) results in rank deficient $\boldsymbol{K}_e$ for polygonal elements with more than eight nodes. In this context, specific characteristics of Voronoi discretisations in combination with PolyFEM can be exploited. In a recent work, (Jayabal & Menzel, 2011), two-dimensional Voronoi discretisations are discussed. In that study, it turned out that the polynomial function for the approximation of stresses that render $\boldsymbol{K}_e$ to be rank sufficient for a quadrilateral element – together with a linear interpolation of the displacements along the element edges – can be used for all polygonal finite elements of the two-dimensional Voronoi-cell-based discretisations. Even though these approximation functions provide rank deficient $\boldsymbol{K}_e$ for elements with more than four, the combination of Voronoi-based meshes and the PolyFEM rendered in the global stiffness matrix to be rank sufficient after incorporation of the boundary conditions. This property has been demonstrated by means of several two-dimensional numerical examples based on Voronoi-generated meshes and different approximation functions for the stresses and displacements (see Jayabal & Menzel, 2011). Such properties, as studied as this work proceeds, may also be expected for the three-dimensional case of Voronoi-cell-based discretisations in combination with the PolyFEM.

3.1. *Determination of $\boldsymbol{J}_e$ and $\boldsymbol{G}_e$*

After discretisation of the domain of interest and selection of the stress approximating function, $\boldsymbol{J}_e$ and $\boldsymbol{G}_e$ are to be determined for each polygonal element to compute $\boldsymbol{K}_e$. As seen in Equations (4b) and (4a), $\boldsymbol{J}_e$ is to be evaluated with respect to the volume of the polygonal element whereas $\boldsymbol{G}_e$ is computed over the boundary of the element.

Each polygonal element in a three-dimensional Voronoi discretisation differs in general in type, shape and size as compared with the rest of the elements of the entire mesh. To give an example, in case one polygonal element consists of only four surfaces, another element may possess more than 20 surfaces. Hence, it is a non-trivial task to determine $\boldsymbol{J}_e$ directly for each element without dividing it into sub-volumes easier to handle. Practically speaking, the total volume of the polygonal finite element can be divided into several standard volumes so that the integration scheme can be set up straightforwardly. In order to establish one and the same algorithm to evaluate $\boldsymbol{J}_e$ for different types of polygonal elements, the following procedure is proposed in this work: the centroid of the volume of a polygonal element, O, and the centroid of one of its surfaces, say P, are calculated. These two points together with any two consecutive corners of the considered surface can be used to construct a tetrahedron. In view of the illustration in Figure 2(a), consider the corners c and d of the element surface $abcdefg$, which form the first tetrahedron $cdPO$. The next two corners d and e form the second tetrahedron $dePO$ and so forth. Hence, the number of tetrahedrons obtained for a given element surface equals the number of edges of that surface. If the element surface is already a triangle, only one tetrahedron needs to be constructed for that surface. This procedure is repeated for all surfaces of the polygonal finite element to obtain the total number of tetrahedrons associated with that element. Finally, $\boldsymbol{J}_e$ is determined for a polygonal element with i tetrahedrons, by

$$\boldsymbol{J}_e = \int_{\mathcal{B}_e} \boldsymbol{M}^{\mathrm{t}} \cdot \mathbf{C}^{\mathrm{voi}} \cdot \boldsymbol{M} \mathrm{d}v = \sum_i \int_{\mathcal{B}_e^i} \boldsymbol{M}^{\mathrm{t}} \cdot \mathbf{C}^{\mathrm{voi}} \cdot \boldsymbol{M} \mathrm{d}v, \tag{10}$$

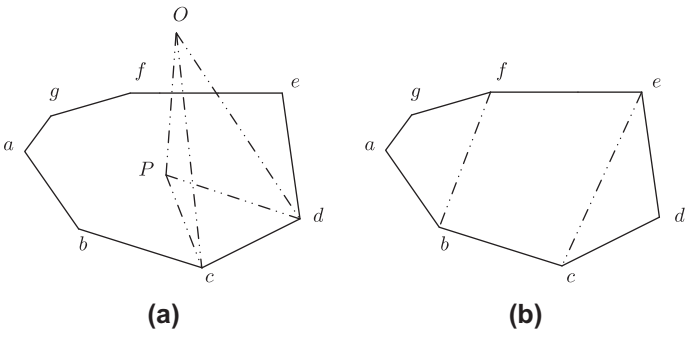

Figure 2. (a) Division of a polygonal finite element into tetrahedrons as $\boldsymbol{J}_e$ is to be evaluated with respect to the volume of the element and (b) division of an element surface into quadrilaterals and triangles as $\boldsymbol{G}_e$ is computed over the boundary of the element.

where $\mathcal{B}_e$ denotes the entire element volume and $\mathcal{B}_e^i$ refers to the volume of i^{th} tetrahedron in that element. Apparently, the tetrahedrons obtained by this subdivision to not take the interpretation as finite elements themselves.

A polygonal finite element consists of polygonal surfaces with a varying number of edges, for instance, from three to 10. Since the matrix $\boldsymbol{G}_e$ is to be determined on the element boundary, it has to be evaluated on each surface of the element and, thereafter, is assembled consistent with the nodal degrees of freedom. One can make use of rather complex integration schemes to evaluate $\boldsymbol{G}_e$ directly on the entire polygonal surface (see Mousavi & Sukumar, 2011). Alternatively, well-established interpolation functions can be applied to simplify the formulation (see Hughes, 1987) among others. This, however, is rather cumbersome for surfaces with more than four edges so that we divide such surfaces into several quadrilaterals and triangles. To give an example, a polygonal surface with seven edges, *abcdef* as shown in Figure 1(b), is divided into three sub-surfaces – two quadrilaterals and one triangular. The matrices $\boldsymbol{G}_e^j$ are evaluated independently on these three sub-surfaces and thereafter added to obtain the contribution of the entire element surface *abcdef* to $\boldsymbol{G}_e$. Conceptually speaking, one polygonal surface face is replaced by several quadrilateral and triangular sub-surfaces, all of them possessing one and the same outward normal unit vector $\boldsymbol{n}$. This procedure is repeated on all polygonal surfaces of the element. Finally, $\boldsymbol{G}_e$ of the entire polygonal element is calculated by summation of all contributions of all surfaces of the element, i.e.

$$\boldsymbol{G}_e = \int_{\partial\mathcal{B}_e} \boldsymbol{M}^{\mathrm{t}} \cdot [\boldsymbol{n} \cdot \boldsymbol{N}] \mathrm{d}a = \sum_j \int_{\partial\mathcal{B}_e^j} \boldsymbol{M}^{\mathrm{t}} \cdot [\boldsymbol{n} \cdot \boldsymbol{N}] \mathrm{d}a, \tag{11}$$

where $\partial\mathcal{B}_e$ refers to the entire element boundary and $\partial\mathcal{B}_e^j$ represents the surface of the j-th polygonal sub-surface.

4. Numerical examples

The three-dimensional Voronoi-based polygonal discretisations used in the following numerical examples are generated by using the Multi-Parametric Toolbox (MPT) in MATLAB. The number of seed points coincides with the number of elements in the Voronoi-cell-based mesh. A random generation of these points is used. In consequence, the Voronoi discretisations discussed in the following are not controlled ones but naturally evolved.

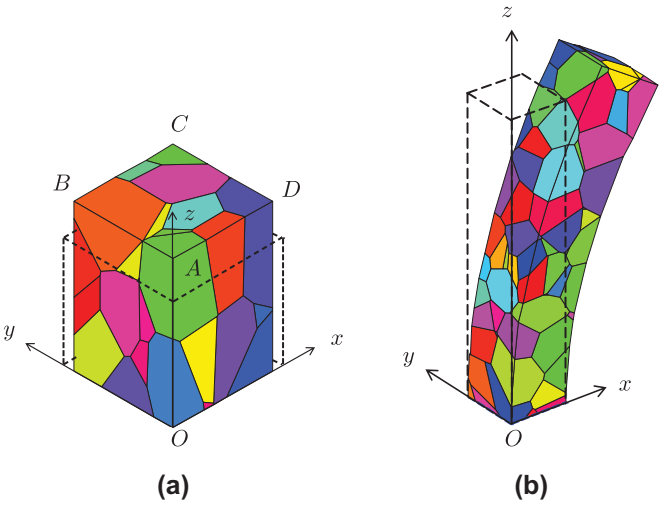

Figure 3. (a) Deformed configuration of a Voronoi-based discretisation with 50 polygonal elements for a tensile loading case. The undeformed boundary of the domain is shown in dashed lines whereas the displacements to display the deformation are magnified by a factor of 500 and (b) deformed configuration of a Voronoi-based discretisation with 100 polygonal elements for a pure bending case. The magnification factor for the displacements to visualise the deformation is 100.

4.1. Tension test

A volume of $1 \times 1 \times 1\,\text{mm}^3$ is discretised by Voronoi-based polygons with the total number of elements chosen as 5, 10, 50, 100 and 200. Homogeneous and isotropic material properties are assigned to all the elements with a Young's modulus E of 30 GPa and a Poisson's ratio v of 0.3.

As homogeneous material properties are assigned to all the elements in the mesh, the displacements are to vary linearly and the strains remain constant in the domain for the case of simple tension considered. Displacement and traction boundary conditions are applied to the discretisation, see also Figure 3(a), namely

$$\begin{aligned} u_x &= 0 \quad \text{at} \quad z = 0 \quad \text{and} \quad x = 0, \\ u_y &= 0 \quad \text{at} \quad z = 0 \quad \text{and} \quad y = 0, \\ u_z &= 0 \quad \text{at} \quad z = 0, \\ \bar{t}_z &= \mathrm{T} \quad \text{at} \quad z = z_{\max}, \end{aligned} \tag{12}$$

where u_x, u_y and u_z refer to the displacements along the x-, y- and z-axes and T denotes a constant in MPa. The displacements are interpolated along the element boundary after dividing these surfaces into quadrilaterals and triangles as discussed in the previous section. The approximation function for the stresses $\boldsymbol{M}$, which in the form provided in Equation (9) makes $\boldsymbol{K}_e$ rank sufficient only for hexahedral elements, is used for all polygonal elements in the Voronoi mesh. This includes, for instance, a polygonal element with 21 surfaces and 38 nodes. As seen in Equation (8), this form of $\boldsymbol{M}$ used here makes $\boldsymbol{K}_e$ rank insufficient for elements with more than eight nodes. However, the global stiffness matrix turns out to possess full rank for all Voronoi-based meshes studied after the boundary conditions are incorporated. Moreover, all individual $\boldsymbol{K}_e$ showed rank-insufficiency for two of the discretisations studied since all elements in these meshes consist of elements with

Table 1 Comparison of the displacements (in μm) between the analytical and the PolyFEM solution for tension loading.

disp	Solution	Point A	Point B	Point C	Point D
u_x	Analytical	0.0	0.0	−0.2	−0.2
	PolyFEM	0.0000	0.0000	−0.2000	−0.2000
u_y	Analytical	0.0	−0.2	−0.2	0.0
	PolyFEM	0.0000	−0.2000	−0.2000	0.0000
u_z	Analytical	0.6667	0.6667	0.6667	0.6667
	PolyFEM	0.6667	0.6667	0.6667	0.6667

more than eight nodes. The global stiffness matrices, however, possess full rank and exact solutions are produced by all Voronoi meshes. To illustrate these results, four points of the discretisations are indicated in Figure 3(a) – to be specific, $A \equiv [0, 0, 1]$, $B \equiv [0, 1, 1]$, $C \equiv [1, 1, 1]$ and $D \equiv [1, 0, 1]$ – to compare their displacements obtained with the PolyFEM with the analytical solutions. Table 1 highlights these patch test type results for a traction of $\mathrm{T} = 20\,\mathrm{MPa}$.

4.2. Bending test

A three-dimensional specimen of $1 \times 1 \times 5\,\mathrm{mm}^3$ – loaded under pure bending – is discretised by Voronoi-cell-based polygons with the total number of elements chosen as 50, 100 and 300. The discretisation with 100 polygonal finite elements is shown in Figure 3(b). When solving such a three-dimensional pure bending linear elastic beam problem, symmetry conditions can be exploited. The analytical solution for the problem at hand can be derived from the elaborations in Timoshenko and Goodier (1970) and for the specified coordinate system one obtains

$$u_x = \frac{\mathrm{T}}{E\, x_{\max}}\left[z^2 + \frac{v}{4}[[x_{\max} - 2x]^2 - 4y^2]\right] \tag{13a}$$

$$u_y = -\frac{\mathrm{T}}{E\, x_{\max}} v\ [x_{\max} - 2x]y \tag{13b}$$

$$u_z = \frac{\mathrm{T}}{E\, x_{\max}}\,[x_{\max} - 2x]z \tag{13c}$$

where T, in MPa, denotes a constant. The analytical solution above is based on fixing the point lying exactly at the middle of the bottom edge along the x-axis, i.e. the point $[\frac{1}{2}x_{\max}, 0, 0]$, in combination with further necessary boundary conditions. In general, such a mid point does not coincide with the position of an element node – in particular for randomly generated Voronoi-cell-based meshes. Hence, the point [0,0,0], denoted by O in Figure 3(b), is fixed for all discretisations used. The boundary conditions applied to solve the bending problem are

$$\begin{aligned} u_y &= 0 \quad \text{at} \quad y = 0 \\ u_z &= 0 \quad \text{at} \quad z = 0 \\ u_x &= 0 \quad \text{at} \quad [x, y, z] = [0, 0, 0] \end{aligned}$$

Table 2 Comparison of the displacements (in μm) between the analytical and the PolyFEM solution for bending loading.

Disp.	Solution	No. of elem.	Point A	Point B	Point C	Point D
u_x	PolyFEM	50	16.3100	16.0818	16.1515	16.1806
		100	16.4516	16.2731	16.2802	16.4769
		300	16.6332	16.4410	16.4349	16.6330
	Analytical		16.7167	16.5167	16.5167	16.7167
u_y	PolyFEM	50	0	−.2213	.2512	0
		100	0	−.1954	.2125	0
		300	0	−.2023	.2025	0
	Analytical		0	−.2000	.2000	0
u_z	PolyFEM	50	3.3475	3.2482	−3.3852	−3.2583
		100	3.3192	3.3441	−3.3350	−3.2819
		300	3.3249	3.3278	−3.3269	−3.3374
	Analytical		3.3333	3.3333	−3.3333	−3.3333

$$\bar{t}_z(x) = \mathrm{T}\left[1 - \frac{2x}{x_{\max}}\right] \quad \text{at} \quad z = z_{\max} \tag{14}$$

By analogy with the simulation of the tension problem, the matrix $\boldsymbol{M}$ defined in Equation (9) is used to approximate the stresses in all the polygonal elements. The displacements are defined on the element boundaries using interpolations pertained to triangle and quadrilateral sub-planes. Since the displacements vary quadratically and bi-linearly in x, y and z – as seen in Equation (13) – refining the mesh should render the numerical results to converge to the analytical solution. Note that the points to generate the Voronoi-based discretisations are randomly chosen. Hence, even a Voronoi mesh generated with a higher number of random

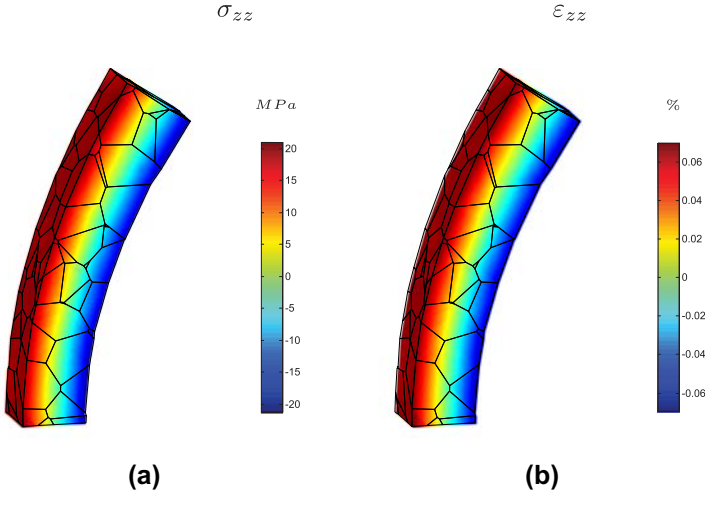

Figure 4. Visualisation of the distribution of (a) the longitudinal stresses σ_{zz} and (b) the longitudinal strains ε_{zz} for a Voronoi-based discretisation with 100 polygonal finite elements under pure bending conditions. The magnification factor for the displacements to visualise the deformed configuration is 100.

points cannot always be expected to possess a finer discretisation in all parts of the body considered. Nevertheless, by further refining the mesh the solution convergences as demonstrated in Table 2 by mean of Voronoi meshes with 50, 100 and 300 elements and for $T = 20\,\text{MPa}$. Four points of the beam are considered – i.e. $A \equiv [0, 0, 5]$, $B \equiv [0, 1, 5]$, $C \equiv [1, 1, 5]$ and $D \equiv [1, 0, 5]$ – to compare the solution based on the PolyFEM with the analytical solutions. The distribution of the stress and strain components along the z-axis is visualised in Figure 4 which is consistent with the analytical results.

5. Summary

In this work, application of a hybrid finite element approach on three-dimensional Voronoi-cell-based discretisations is studied for linear elastic mechanical problems. Several details of the algorithmic implementations of the method are discussed in detail. Specific advantages of employing Voronoi-based meshes in the context of a polygonal finite element approach is highlighted. In this regard, ensuring rank-sufficiency conditions for every individual element stiffness matrix in the Voronoi meshes appears not necessary. The stress approximation function adequate to make a hexahedral element rank sufficient may be used for all types of polygonal finite elements, independent of the number of element nodes. The global stiffness matrix would turn out rank-sufficient, after incorporation of the boundary conditions, even though individual element stiffness matrices might be rank-insufficient. Such an implementation considerably reduces the computational cost when applying the PolyFEM in combination with Voronoi-cell-based meshes. These relations appear to hold for naturally evolving Voronoi meshes, i.e. the meshes generated using random seed points. For specific types of Voronoi-based polygonal meshes, for example with regular polyhedrons, further investigation should be carried out as the result mentioned above may in general not apply. The PolyFEM can be extended to coupled problems, such as the simulation of piezoceramic materials wherein the grains present in the polycrystalline micro-structure are modelled by individual polygonal finite elements with anisotropic material properties (Jayabal & Menzel, 2012). A further extension of the formulation can include so-called domain switching process in ferroelectrics at the micro-structural level of grains, respectively, domains. With regard to such material modelling, the main advantage of the PolyFEM is its ability to represent the geometry of an individual grain by one polygonal finite element, which could make this method computationally efficient.

References

Aurenhammer, F. (1991). Voronoi diagrams – a survey of a fundamental geometric structure. *AMC Computing Surveys, 23*, 345–405.

Ghosh, S., & Mallett, R.L. (1994). Voronoi cell finite elements. *Computers & Structures, 50*, 33–46.

Ghosh, S., & Moorthy, S. (1995). Elastic-plastic analysis of arbitrary heterogeneous materials with the Voronoi cell finite element method. *Computer Methods in Applied Mechanics and Engineering, 121*, 373–409.

Ghosh, S., & Moorthy, S. (2004). Three dimensional Voronoi cell finite element model for microstructures with ellipsoidal heterogeneties. *Computational Mechanics, 34*, 510–531.

Hughes, T.J.R. (1987). *The finite element method*. Prentice-Hall.

Jayabal, K., & Menzel, A. (2011). Application of polygonal finite elements to two-dimensional mechanical and electro-mechanically coupled problems. *Computer Modeling in Engineering & Sciences, 73*, 183–208.

Jayabal, K., & Menzel, A. (2012). Voronoi-based three-dimensional polygonal finite elements for electro-mechanical problems. *Computational Materials Science*. doi : 10.1016/j.commatsci.2012.02.049.

Jayabal, K., Menzel, A., Arockiarajan, A., & Srinivasan, S.M. (2011). Micromechanical modelling of switching phenomena in polycrystalline piezoceramics: Application of a polygonal finite element approach. *Computational Mechanics, 48*, 421–435.

Mousavi, S.E., & Sukumar, N. (2011). Numerical integration of polynomials and discontinuous functions on irregular convex polygons and polyhedrons. *Computational Mechanics, 47*, 535–554.

Pian, T.H.H. (1964). Derivation of element stiffness matrices by assumed stress distribution. *American Institute of Aeronautics and Astronautics, 2*, 1333–1336.

Sze, K.Y., & Sheng, N. (2005). Polygonal finite element method for nonlinear constitutive modeling of polycrystalline ferroelectrics. *Finite Elements in Analysis and Design, 42*, 107–129.

Timoshenko, S.P., & Goodier, J.N. (1970). *Theory of elasticity*, 3rd ed. New York: McGraw-Hill.